

Squeezing-Enhancement of Stimulated and Spontaneous Raman Spectroscopy

YOAD MICHAEL,¹ LEON BELLO,¹ MICHAEL ROSENBLUH,¹ AND AVI PE'ER^{1,*}

¹*Department of Physics and BINA Center for Nanotechnology, Bar-Ilan University, Ramat Gan 5290002, Israel*

**avi.peer@biu.ac.il*

Abstract: The sensitivity of coherent Raman spectroscopy methods, such as Coherent Anti-Stokes Raman Spectroscopy (CARS) or Stimulated Raman Spectroscopy (SRS), is ultimately limited by shot-noise from the stimulating fields. We present a squeezing-enhanced Raman spectroscopy scheme that achieves sub-shot-noise sensitivity, along with enhancement of the Raman gain, and inherent background suppression. Our configuration incorporates the Raman sample between two parametric amplifiers that squeeze the light along orthogonal quadrature axes, such that all light created by the first amplifier is annihilated by the second amplifier, forming a nonlinear SU(1,1) interferometer. The Raman response in the sample induces a phase shift to signal-idler frequency-pairs within the fingerprint spectrum of the molecule, resulting in a signal that is proportional to the Raman response of the sample multiplied by the squeezing factor of the parametric amplifiers. Seeding the interferometer with coherent input further stimulates the Raman signal classically without increasing the background, effectively forming a squeezing-enhanced version of CARS, where the squeezing enhancement is achieved on top of the classical stimulation.

© 2025 Optical Society of America

1. Introduction

Raman scattering is widely used for major sensing applications, such as Raman spectroscopy [1], microscopy [2] and material study [3] due to its ability to identify the molecular contents of a sample based on its Raman fingerprint spectrum, which reflects the unique vibrational and rotational structure of each molecule. Raman spectroscopy is therefore an ideal contrasting method for chemically resolved microscopy [4] [5] with no need for prior preparation or fluorescent tagging of the target molecule. The major challenge of Raman sensing is the relative weakness of the Raman response, which is several orders of magnitude weaker than fluorescence, and is often obscured by other light-matter interactions. For this reason, much effort was invested in the past to improve the observed Raman signal in variations of Stimulated Raman Scattering (SRS) [6] and Coherent Anti-Stokes Raman Scattering (CARS) [7] [8].

In standard CARS, a Raman sample is excited by a strong pump wave (frequency ω_p) and a Stokes wave (idler, frequency ω_i) that interact within the sample to generate an anti-Stokes (signal) wave at frequency $\omega_s = 2\omega_p - \omega_i$ via Four-Wave Mixing (FWM). When the frequency difference between the pump and Stokes field matches a molecular vibration/rotation in the sample, the generated anti-Stokes field is resonantly enhanced, indicating that the Raman shift of the signal (with respect to the pump) acts as a molecular fingerprint. However, since FWM is a parametric process, non-resonant FWM through virtual levels can also occur, where the frequency difference between the pump and Stokes waves does not correspond to a vibrational transition of the molecule, resulting in a non-resonant background that is not chemically specific. In pure or highly-concentrated samples this background usually does not pose a problem, since the non-resonant response is much weaker than the resonant one, but in diluted samples, where the target molecule is surrounded by large quantities of background molecules (e.g. protein dissolved

in water within a biological cell), the non-resonant background from the environment can become a major limiting factor, since it dominates and obscures the weak resonant Raman signal from the target molecule (protein). The fundamental limit to the sensitivity of standard CARS is therefore the noise associated with the non-resonant background, indicating that suppression of this background is a major goal for CARS spectroscopy with several methods proposed in the past to address it. For example, pulse shaping was applied to reduce the peak power of the exciting pulses [9] (and hence the non-resonant background), epi-CARS that detects only the back-scattered Raman signal [10] (which is primarily resonant), and polarization CARS that rejects the non-resonant signal based on polarization [11]. These methods are not always general, since they rely on some specific property of the sample/light to suppress the background, and remain limited by shot-noise (even with ideal background suppression), which is the ultimate limitation of classical detection methods.

We suggest a highly general Raman configuration (Fig. 1b) that excites the sample with squeezed coherent light and enhances the Raman gain of the sample by the squeezing ratio, while completely rejecting the non-resonant background based on the fundamental difference between resonant and nonresonant excitations. The broadband two-mode squeezed light is generated via FWM in an optical parametric amplifier (OPA), and probes the Raman interaction in the sample, which is also a weak FWM process on its own, while taking advantage of the nonclassical quantum correlation properties of the squeezed illumination [12]. Due to the inherent phase shift between resonant and non-resonant interactions, and the phase sensitivity of the FWM process [13], the non-resonant background can be completely eliminated (beyond the shot noise limit), forming a quantum analog of interferometric CARS [14] [15], as explained hereon.

Our analysis of this squeezing-enhanced Raman spectroscopy method is organized as follows: Section 1 shortly reviews the SU(1,1) interferometer, and how the squeezed illumination enables sub-shot-noise interferometric phase detection. Section 2 analyzes the ideal simple case of a resonant, narrowband Raman sample (a weak parametric amplifier) that is placed inside a lossless SU(1,1) interferometer. We calculate the output intensity of the signal as a function of the gain of both the Raman sample and the OPA, which highlight the squeezing enhancement of the resonant Raman signal. Section 3 analyses the additional effect of non-resonant interaction in the Raman sample, demonstrating how the non-resonant background can be discriminated from the resonant term and completely eliminated due to the inherent $\pm\pi/2$ phase shift between resonant and nonresonant interactions. Section 4 introduces coherent seeding of the interferometer by classical fields, effectively forming a squeezing-enhanced version of standard CARS, where the squeezing enhancement of section 2 is achieved on top of the classical stimulation of the Raman interaction with a coherent idler. Finally, Section 5 incorporates loss in the analysis, either internal or external to the interferometer, which is a critical consideration for experimental realizations of any squeezing application, showing that the squeezing-enhancement beyond the shot-noise limit survives with practical levels of loss.

2. Analysis

2.1. Standard SU(1,1) Interferometric detection

Interferometric measurements allow for highly sensitive detection of any physical phenomenon that induces an optical phase shift. The phase sensitivity of interferometric schemes depends on both the illumination source and the configuration of the interferometer: Standard SU(2) interferometers, such as the Michelson or Mach-Zehnder, achieve a phase sensitivity of $1/\sqrt{N}$ - the shot-noise limit, when fed with coherent light [16] (N the number of photons that traversed the interferometer during the detection period). SU(2) interferometers can surpass this limit when the unused port of the interferometer is fed with squeezed light [17], as utilized for example in LIGO for detection of gravitational waves [18]. The SU(1,1) nonlinear interferometer (Fig. 1a) is a fundamentally different type of interferometric detector, where nonlinear gain media

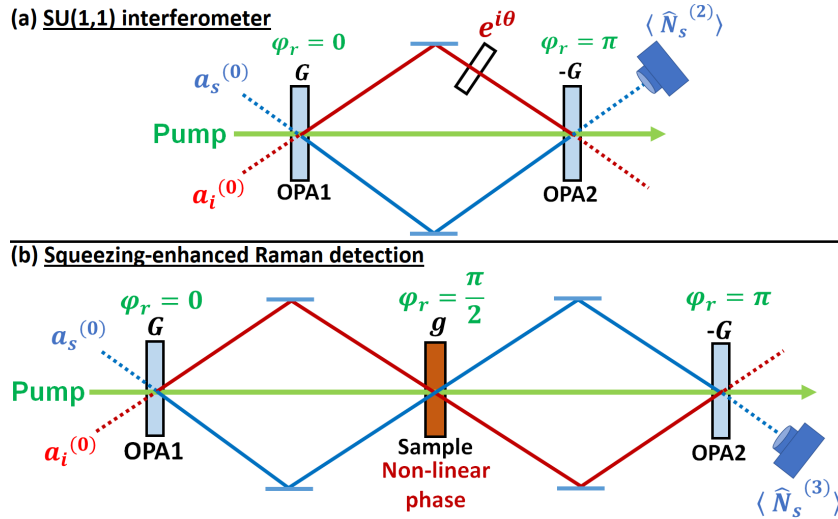


Fig. 1. Squeezing-enhanced Raman detection in an SU(1,1) interferometer. a) The standard SU(1,1) interferometric detection of a linear phase: Two OPAs of equal gain and opposite pump phases are arranged in series (balanced configuration). The 1st OPA amplifies signal-idler pairs at the input (seeded or vacuum), while the 2nd OPA is shifted in pump phase to exactly reverse the amplification of OPA1 and return the light back to its original input state, nulling the intensity of the signal and idler at the output. When a linear phase shift θ is introduced between the amplifiers, the cross-cancellation of the amplifiers is no longer complete, thereby detecting the phase with sub-shot-noise sensitivity due to the squeezing of the OPAs. b) Our scheme for squeezing-enhanced Raman detection: The Raman sample is introduced inside a balanced SU(1,1) interferometer. The sample acts as a weak parametric amplifier whose relative phase is set to $\phi_r = \pi/2$, effectively shifting the phase within the interferometer and elevating the dark level of the output light, as explained in the text.

(OPAs) replace the beam splitters, and squeezed light is generated within the interferometer itself without the need to feed it externally. Additionally, the SU(1,1) interferometer can be robust to detection losses, as discussed by Lett [19] and Chekhova [20] [21].

In a parametric process (which occurs in both OPA1 and OPA2, as marked in Fig. 1a), the direction of energy transfer - from the pump to the signal and idler or vice-versa - depends on the relative phase $\phi_r = 2\phi_p - (\phi_i + \phi_s)$ between the pump and a signal-idler pair, such that either amplification ($\phi_r = 0$) or attenuation ($\phi_r = \pi$) of the signal-idler pair occurs. In the field-quadrature picture, each OPA amplifies one quadrature component of the combined signal-idler field and attenuates the other quadrature component according to the phase of the pump, thereby squeezing the input [22] [23] [24].

Consider the two OPAs of the SU(1,1) interferometer arranged in series with equal gain in a "crossed" configuration, where the attenuation axis of OPA2 matches the amplification axis OPA1 and vice-versa (setting $\phi_r = 0$ in OPA1 and $\phi_r = \pi$ in OPA2). Thus, the output quantum state of the light remains unchanged from the input, as OPA2 exactly reverses the squeezing of OPA1. Yet, if the phase of the light is altered between the amplifiers, the cancellation will not be complete, leading to an interferometric detection of the induced phase. Indeed, when the standard SU(1,1) interferometer measures a linear phase shift θ between the two OPAs (assuming vacuum input for now), the number of signal (or idler) photons at the output is given by:

$$\langle \hat{N}_s \rangle_{SU(1,1)} = \frac{1}{2} \sinh^2(2G) \cdot (1 - \cos(\theta)), \quad (1)$$

where G is the gain of the OPAs. If no phase shift is present, the output is vacuum (identical to the input), where both first and second moments of the photon number are zero ($\langle \hat{N}_s \rangle, \langle \hat{N}_s^2 \rangle = 0$), allowing signal detection, which is background-free. The phase sensitivity (as was previously discussed in [16] [25] [26]) is given by:

$$\theta_{min} = \frac{1}{\sinh(2G)} \approx \frac{1}{N_{sq}}, \quad (2)$$

where N_{sq} is the number of squeezed signal and idler photons generated inside the interferometer. The result of Eq.2 shows sub-shot-noise scaling, allowing for super sensitive phase detection (ideally Heisenberg sensitivity of $1/N_{sq}$).

2.2. The ideal squeezing-enhanced Raman scheme

In the previous section, we reviewed the sub-shot-noise phase sensitivity of the standard SU(1,1) interferometer. In our scheme for enhanced Raman spectroscopy, shown in Fig. 2a, the Raman sample, which can be considered as a weak parametric amplifier via FWM, is placed inside an SU(1,1) interferometer, where the squeezed signal and idler pairs generated in OPA1 (with a relative phase $\phi_r = 0$) interact parametrically in the Raman sample at an intermediate phase $\phi_r = \pi/2$, which translates to an amplification axis of 45° and causes rotation of the squeezing ellipse - an effective phase shift (see Fig. 2b). OPA2 then amplifies at an opposite relative phase $\phi_r = \pi$, which reconverts the signal-idler pairs back to pump light, and detects the nonlinear phase shift induced by the sample via the changes of the signal intensity at the output.

Let us now calculate the light intensity (number of photons) at the output of the squeezing-enhanced Raman configuration. When passing through the amplifiers (and the sample), we can use the input-output relation of each amplifier:

$$\hat{a}_{s,i}^{(1)} = A\hat{a}_{s,i}^{(0)} + B\hat{a}_{i,s}^{\dagger(0)}, \quad (3)$$

$$\hat{a}_{s,i}^{(2)} = C\hat{a}_{s,i}^{(1)}e^{i\pi/4} + D\hat{a}_{i,s}^{\dagger(1)}e^{-i\pi/4}, \quad (4)$$

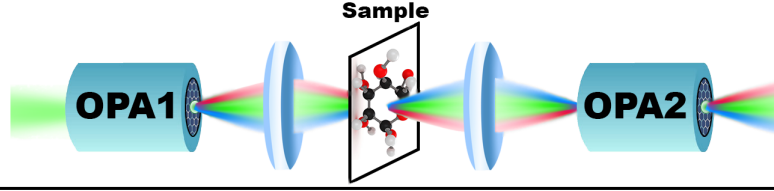
$$\hat{a}_{s,i}^{(3)} = A\hat{a}_{s,i}^{(2)}e^{i\pi/4} + B\hat{a}_{i,s}^{\dagger(2)}e^{-i\pi/4}, \quad (5)$$

where A and B are parameters associated with the gain of the OPAs: $A = \cosh(G)$ and $B = i \sinh(G)$, with G the gain of the amplifiers and C and D are associated with the gain of the Raman sample, $C = \cosh(g_r)$ and $D = i \sinh(g_r)$ with g_r the gain of the Raman sample (assumed for now to be purely resonant and narrowband). The relative phase between the pump, signal and idler varies throughout the different amplifiers, and is adjusted such that the two OPAs are orthogonal to each other. Thus, we apply a $\pi/4$ phase to both the signal and idler fields twice: first after OPA1, which rotates the sample itself to a 45° amplification axis ($\phi_r = \pi/2$), and a second $\pi/4$ after the sample, which sets OPA2 orthogonal to OPA1 ($\phi_r = \pi$).

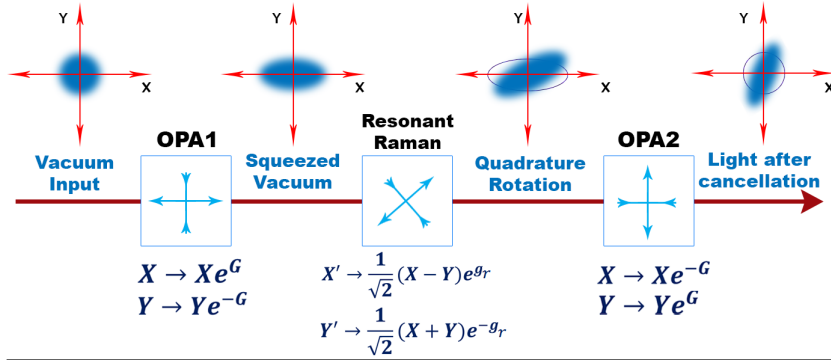
Note that although the external amplifiers are always set orthogonal to each other, the Raman response of the sample is generally complex with respect to the pump drive, and its phase varies spectrally across the resonance from $\phi_r = 0$ below resonance, through $\phi_r = \pi/2$ on resonance to $\phi_r = \pi$ above resonance. Generally speaking, the imaginary part of the Raman response is associated with the absorption, which is maximal on resonance, whereas the real part of the response is associated with dispersion, which is nulled on resonance, just like a driven two-level system [27]. This section analyzes the sample response on resonance, while the non-resonant response is analyzed in the next section.

The total relative phase for the FWM light before OPA2 is $\phi_r = \pi$, indicating that without a sample ($C = 1, D = 0$), the scheme is reduced to the standard SU(1,1) interferometer with

(a) **Squeezing enhanced Raman scheme**



(b) **Resonant interaction in the Raman sample**



(c) **Non-resonant interaction in the Raman sample**

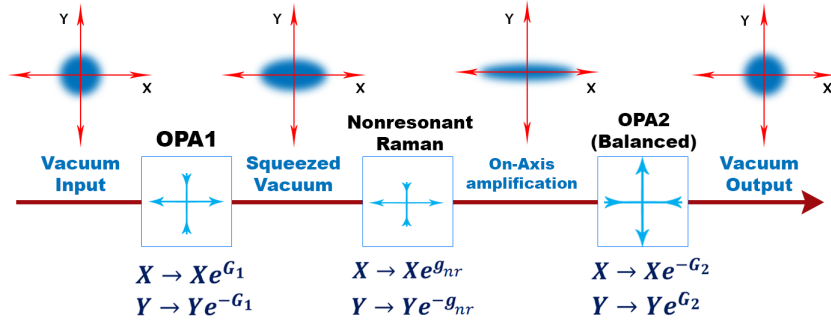


Fig. 2. Overview of the signal-idler quadratures within the squeezing-enhanced Raman configuration. (a) Conceptual illustration of the scheme, where photonic crystal fibers represent the OPAs. (b) and (c) show the quadrature dynamics of the light throughout the different amplifiers for resonant and non-resonant interactions respectively. The top line of graphs in (b) and (c) portrays the quadrature map of the two-mode light at various locations along the interferometer, and the bottom part shows amplification/attenuation axes of each amplifier (indicated by arrows pointing outwards/inwards). OPA1 and OPA2 are set in a crossed (orthogonal) configuration. In the resonant case (b), the Raman sample is set at 45° , which rotates the quadrature axes between the OPAs, resulting in light at the output. The transparent ellipses/circles illustrate the state of the light in the absence of a sample, where the output returns exactly to to the input state (vacuum). (c) For a non-resonant Raman sample the interaction is $\pi/2$ shifted with respect to the resonant case, indicating that the amplification axis of the sample remains aligned with the external OPAs, and the signal does not undergo quadrature rotation. Rather, the non-resonant gain g_{nr} unbalances the interferometer by effectively increasing/decreasing the gain of OPA1 G_1 . This contribution can be completely negated by tuning the gain of OPA2 to $G_2 = G_1 + g_{nr}$.

complete destructive interference. With the Raman sample in, a nonlinear phase shift is induced, and the photon number of the signal at the output is (see Supplementary material for derivation):

$$\begin{aligned} \langle \hat{N}_s^{(3)} \rangle &= |D|^2(|A|^2 + |B|^2 + 2|A||B|) \\ &= \sinh^2(g_r) \cdot \cosh^2(2G). \end{aligned} \quad (6)$$

Eq.6 demonstrates the enhancement of the Raman gain in the sample due to its interaction with the squeezed light generated by the interferometer. We can compare the result of Eq.6 to that of spontaneous Raman emission: $\langle \hat{N}_s^{(3)} \rangle = \sinh^2(g_r)$, which corresponds to setting the OPA gain to zero $G = 0$. Thus, Eq. 6 illustrates the coupling between the parameters of the sample (C, D, g_r) and the parameters of the crossed amplifiers (A, B, G), creating an effective squeezing-enhanced gain, but with no added background (the non-resonant background can be eliminated by rearranging the gain of the external OPAs, as explain in the next section). Thus, although the sample is stimulated by the FWM light of OPA1, the interferometer "conceals" this stimulation completely, acting as an effective "black-box", which to an external observer appears as a spontaneous Raman scatterer, but with a higher (squeezing-enhanced) gain. As explained in section 4, this effective "black-box" remains applicable also for stimulated Raman techniques as well, such as SRS and CARS, where seeding the crossed interferometer configuration with a coherent idler results of a signal analogous to standard CARS, but with the enhanced Raman gain due to the squeezed illumination within the interferometer and elimination of the background, as explained hereon.

2.3. Complete suppression of the non-resonant background

In the previous section, we considered only the contribution of the resonant Raman process to the output intensity. The non-resonant background of the sample, which we discuss here, arises from dispersive interaction with other molecules in the sample, which is inherently phase shifted by $\pm\pi/2$ with respect to the resonant signal (as with any oscillator that is driven off resonance) [28]. Thus, we should treat the Raman sample as a parametric amplifier capable of two separate amplifications: It simultaneously performs both the resonant, phase-shifting amplification at $\phi_r = \pi/2$ (discussed thus far) and an additional non-resonant, non-phase shifting on-axis amplification at $\phi_r = 0, \pi$, as shown in Fig. 2c. This amplification behaves as a direct extension to the gain of OPA1, since it amplifies the same quadrature (the same relative phase), indicating that the non-resonant contribution can be completely nulled by a slight variation of the gain of either OPA2 or OPA1. This concept is similar to the experiments of Lupke [29] and Lee [30], where the non-resonant background of the sample was canceled by placing an additional FWM medium after the sample, which generated non-resonant background that destructively interfered with the background from the sample. In our scheme we exploit this background cancellation in combination with the interferometer squeezing to enhance the Raman gain with no added background.

Let us consider a purely non-resonant sample (i.e. a sample whose vibrational resonance Ω does not match the frequency difference between the pump and the idler or signal $\Omega \neq 2\omega_p - \omega_{i,s}$): after passing through OPA1 (with gain G_1), the sample performs non-resonant on-axis (compared to OPA1) amplification at a gain g_{nr} . OPA2 is set as before to negate the amplification of OPA1, this time with gain $G_2 \neq G_1$. The number of photons at the output is:

$$\langle \hat{N}_s^{(3)} \rangle_{nr} = \sinh^2(G_1 + g_{nr} - G_2). \quad (7)$$

Setting the gain of OPA2 to $G_2 = G_1 + g_{nr}$ will null the non-resonant output completely.

In practice, real Raman samples will have both resonant Raman gain from the molecule of interest and non-resonant gain from background molecules (e.g solvent). We can think of the

sample as a mixture of many infinitesimally low gain parametric amplifiers that perform resonant amplification at 45° and non-resonant amplification at 0° with some arbitrary ordering. The resonant and non-resonant gains obviously do not commute, but since the gain of the entire sample is small compared to the OPAs ($g_{nr}, g_r \ll G$), it is fair to assume that the cross-interaction between the resonant and non-resonant gain within the sample ($\sinh^2(g_r) * \sinh^2(g_{nr})$) is negligible compared to the interaction of the sample with the external OPAs. Thus, we may treat the sample as two separate parametric amplifiers (resonant and non-resonant) that are placed in a series, indicating that the non-resonant background can be eliminated by balancing the gain of the interferometer (Eq.7), which yields the photon number at the output:

$$\begin{aligned} \langle \hat{N}_s^{(4)} \rangle &= \sinh^2(g_r) \cosh^2(2(G_1 + g_{nr})) \\ &= \sinh^2(g_r) \cdot \cosh^2(2G_2), \end{aligned} \quad (8)$$

which remains identical to the result of Eq.6, even in the presence of the non-resonant background, which is now fully suppressed (note that $g_{nr} \ll G$, indicating that $G \approx G_1 \approx G_2$ also after gain balancing). In the upcoming sections, we can therefore assume that the non-resonant contribution is cancelled by gain balancing.

2.4. Coherent seeding of the interferometer: Squeezing-enhanced CARS

In standard (non-interferometric) CARS, a Raman sample is seeded with coherent idler light (in addition to the pump), enhancing the Raman response at the signal frequency by classical stimulation of the FWM interaction. The input state for the signal field is vacuum $|0\rangle_s$ and a strong coherent state $|\alpha\rangle_i$ for the idler. The intensity of the output signal in standard CARS is given by:

$$\langle \hat{N}_s \rangle_{CARS} = |D|^2(1 + |\alpha_i|^2) = \sinh^2(g)(1 + |\alpha_i|^2), \quad (9)$$

where $|\alpha_i|^2$ is the intensity of the idler (average number of seed idler photons at the input) and $|D|^2$ is associated with the gain of the sample. However, as noted in the previous section, both g and D may contain contribution from the resonant (D_r) and the non-resonant (D_{nr}) response, which both scale in proportion to $|\alpha_i|^2$, resulting in higher observed signal but not in increased sensitivity. In fact, the noise associated with the non-resonant background is even higher than standard shot-noise, indicating that the sensitivity of standard CARS is even worse than spontaneous Raman unless the non-resonant background is suppressed.

Let us now examine the CARS response of our squeezing-enhanced Raman configuration from subsection 2.2 by subjecting it to a strong coherent idler input. Note first that by simple extension of the treatment in subsection 2.3, we may still assume that the non-resonant background is suppressed by gain balancing the external OPAs, and consider only the resonant response (the stimulation affects both the OPAs and the sample in the same manner, leaving the gain balancing unchanged). This assumption holds true regardless of the input state of the signal or idler. The output photon-number $\langle \hat{N}_s^{(3)} \rangle$ for the seeded configuration $|0_s, \alpha_i\rangle$ (vacuum signal, and strong coherent state for the idler) is then

$$\langle \hat{N}_s^{(3)} \rangle = \cosh^2(2G) \sinh^2(g_r)(1 + |\alpha_i|^2), \quad (10)$$

which is directly equivalent to the expression of Eq. 9 for standard CARS with the additional enhancement of the Raman gain due to the squeezing in the interferometer, and with inherent suppression of the non-resonant background. Consequently, the 'Raman black-box' concept, which claims that the interferometer can behave exactly like a normal Raman sample but with an enhanced gain due to the squeezing, extends also to stimulated interactions. The squeezing effect on the sample appears only internally between the crossed OPAs, but does not leave a

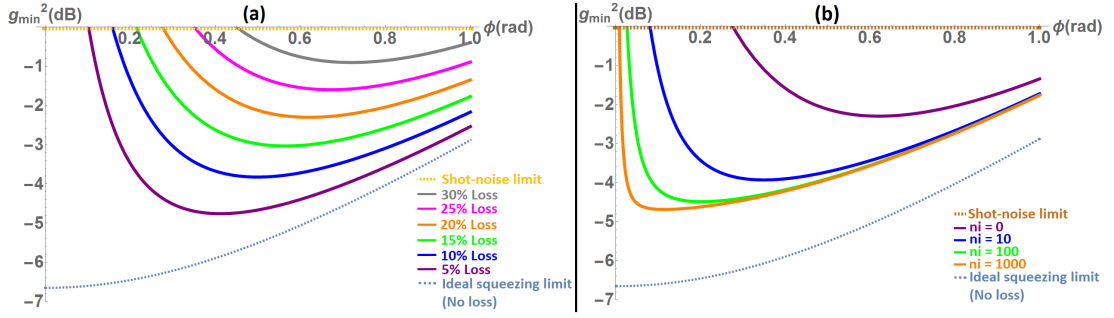


Fig. 3. Sensitivity of the squeezing-enhanced Raman scheme compared to the shot-noise limit, for two different signal-idler inputs: (a) vacuum, and (b) seeded by a coherent idler, where the gain of the OPAs is fixed at a moderate level of $G = 0.7$ (6.8dB of squeezing). The minimum detectable Raman gain in the sample (relative to the shot-noise limit) is shown for various configurations of seeding and internal loss as a function of the phase of OPA2 (at $\phi = 0$ the OPAs are exactly crossed). (a) shows the sensitivity of the unseeded scheme relative to spontaneous Raman spectroscopy (0dB) with various loss values, indicating that sub-shot noise sensitivity can be obtained with practical levels of loss (up to 30%). (b) shows the sensitivity of a Raman interferometer with a fixed internal loss (20%) when seeded with various intensities of a coherent idler ($|\alpha_i|^2 = 0, 10, 100, 1000$). Note that all sensitivities are shown relative to the shot-noise limit at their specific seeding level ($1/\sqrt{|\alpha_i|^2}$). Clearly the seeded configuration maintains substantial reduction below the shot-noise limit with practical levels of loss (showing even improvement over the unseeded case).

trace externally. An external observer will not be able to differentiate the ideal interferometer configuration (without internal loss) from a simple, high-gain resonant Raman sample (unless he can 'look inside the box').

2.5. Detection sensitivity in the presence of loss

We now evaluate the sensitivity of measurement under practical conditions for our suggested scheme by calculating the minimum resonant Raman gain g_{min} of the sample that can be detected in the presence of photon-loss. This sensitivity can be calculated by error propagation analysis:

$$g_{min}^2 = \frac{\langle \hat{N}_s^2 \rangle - \langle \hat{N}_s \rangle^2}{\left| \frac{d}{dg} \langle \hat{N}_s \rangle \right|_{g=0}^2}, \quad (11)$$

which states that the minimum detectable variation of the signal must be comparable to the noise of the output intensity.

For the ideal configuration, where no losses are present, the sensitivity is (See supplemental material):

$$g_{min}^2 = \frac{1}{4 \cosh^2(2G) \cdot (1 + |\alpha_i|^2)}, \quad (12)$$

which is nearly identical to the minimum detectable phase of the standard SU(1,1) interferometer of Eq. 2 (for the unseeded case), and indicates the detection of a single output photon during the finite measurement time.

Both internal loss (between the two OPAs) and external/detection loss (after the interferometer) affect the sensitivity of measurement, although in a different manner. External loss takes place after the nonlinear interference and does not affect the squeezing, therefore reducing the measured signal by a loss factor $|r_{ext}|^2$, identical to the effect of losses on classical light [31]. Internal

loss on the other hand, hinders the quantum correlation between the signal and idler, effectively diminishing the squeezing [23], which in turn degrades the contrast of the nonlinear interference and elevates the dark fringe level (and its associated noise), resulting in a lower detection sensitivity.

Let us calculate the average photon number and the noise associated with the dark fringe (background) due to internal losses for the crossed amplifiers ($\phi = 0$). We use the standard modeling of loss as a beam splitter (BS) placed inside the interferometer [32], where vacuum may enter through the unused port of the BS. We apply the BS loss to the ideal squeezing-enhanced Raman scheme, seeded with a strong (classical) coherent state $|\alpha_i\rangle$ for the idler, and obtain for the resonant signal:

$$\langle \hat{N}_s^{(4)} \rangle = |t|^2 \sinh^2(g) \cdot \cosh^2(2G) \cdot (1 + |\alpha_i|^2) + |r|^2 \sinh^2(G), \quad (13)$$

where r represents the loss and t the transmission inside the interferometer ($|r|^2 + |t|^2 = 1$). Eq. 13 shows two contributions to the measured signal at the output: the resonant Raman signal (left), which is similar to the lossless case, reduced by a transmission coefficient $|t|^2$, and the loss term (right, proportional to $|r|^2$) which corresponds to vacuum amplification by OPA2, and causes direct elevation of the dark fringe level. Since this term does not depend on the Raman sample, it limits the sensitivity of the measurement. In order to distinguish the Raman signal from the dark-fringe background due to the loss, we must consider the noise associated with the background (see Supplemental material):

$$\begin{aligned} \sigma_{loss} &= \sqrt{\langle \hat{N}_s^2 \rangle_{loss} - \langle \hat{N}_s \rangle_{loss}^2} \\ &= \frac{1}{2} |r|^2 \sinh(2G). \end{aligned} \quad (14)$$

Eq.14 represents the background noise of the dark fringe, which limits the ability to detect a small Raman signal. Note that plugging Eq.14 and Eq.13 into Eq.11 results in a diverging expression for g_{min}^2 , and therefore the optimal working point of the interferometer (defined as the relative phase between the OPAs where the sensitivity is optimal) may vary with the internal loss. This behavior is shown in Fig. 3a, which presents the minimum detectable Raman gain as a function of phase between the OPAs for various loss values. For no loss, the optimal working point is $\phi_{opt} = 0$ (exactly crossed amplifiers), as expected. Once loss is introduced, ϕ_{opt} increases due to the dark fringe noise. The squeezing enhancement still improves the minimum detectable signal below the shot-noise limit even in the presence of mild losses, demonstrating the resilience of this scheme to loss. Fig. 3b introduces seeding of the idler port for various intensities (number of photons) with 20% loss. The stimulation appears to somewhat compensate for the effect of loss, and improve the sensitivity plot in two ways: It pushes the optimal phase ϕ_{opt} towards the ideal case $\phi_{opt} = 0$ and also improves the optimal sensitivity (though not all the way to the ideal lossless level). This improvement is primarily because the seeding also stimulates the external OPAs to generate more signal-idler photon pairs, thereby increasing the total number of photons that probe the sample.

3. Conclusions

We presented a method for Raman spectroscopy, which utilizes the squeezed light inside a nonlinear interferometer for enhancement of the resonant Raman signal and for suppression of the non-resonant background in a general Raman sample. This scheme can be treated as a "Raman black box" that can be used to supplement standard Raman techniques, demonstrating a classical stimulation of the signal on top of the squeezing-enhanced gain. This improvement of Raman spectroscopy may find future usage in demanding spectroscopy applications [33], such as explosive detection [34].

Funding

This research was supported by grant No.44/14 from the Israel Science Foundation (FIRST program for high-risk high-gain research).

Acknowledgments

We are grateful to Jose Luis Gomez-Munoz and Francisco Delgado for their "Quantum notation" add-on to the Mathematica software.

References

1. E. B. Hanlon, R. Manoharan, T.-W. Koo, K. E. Shafer, J. T. Motz, M. Fitzmaurice, J. R. Kramer, I. Itzkan, R. R. Dasari, and M. S. Feld, "Prospects for in vivo raman spectroscopy," *Phys. Medicine & Biol.* **45**, R1–R59 (2000).
2. A. Zumbusch, G. R. Holtom, and X. S. Xie, "Three-dimensional vibrational imaging by coherent anti-stokes raman scattering," *Phys. Rev. Lett.* **82**, 4142–4145 (1999).
3. A. C. Ferrari and D. M. Basko, "Raman spectroscopy as a versatile tool for studying the properties of graphene," *Nat. Nanotechnol.* **8**, 235–246 (2013).
4. C. W. Freudiger, W. Min, B. G. Saar, S. Lu, G. R. Holtom, C. He, J. C. Tsai, J. X. Kang, and X. S. Xie, "Label-free biomedical imaging with high sensitivity by stimulated raman scattering microscopy," *Science* **322**, 1857–1861 (2008).
5. J. P. Pezacki, J. A. Blake, D. C. Danielson, D. C. Kennedy, R. K. Lyn, and R. Singaravelu, "Chemical contrast for imaging living systems: molecular vibrations drive cars microscopy," *Nat. Chem. Biol.* **7**, 137–145 (2011).
6. W. J. Tipping, M. Lee, A. Serrels, V. G. Brunton, and A. N. Hulme, "Stimulated raman scattering microscopy: an emerging tool for drug discovery," *Chem Soc Rev.* **45**, 2075–2089 (2016).
7. S. Roy, J. R. Gord, and A. K. Patnaik, "Recent advances in coherent anti-stokes raman scattering spectroscopy: Fundamental developments and applications in reacting flows," *Prog. Energy Combust. Sci.* **36**, 280–306 (2010).
8. R. F. Begley, A. B. Harvey, and R. L. Byer, "Coherent anti-stokes raman spectroscopy," *Appl. Phys. Lett.* **25**, 387–390 (1974).
9. N. Dudovich, D. Oron, and Y. Silberberg, "Single-pulse coherently controlled nonlinear raman spectroscopy and microscopy," *Nature* **418**, 512–514 (2002).
10. A. Volkmer, J.-X. Cheng, and X. S. Xie, "Vibrational imaging with high sensitivity via epidetected coherent anti-stokes raman scattering microscopy," *Phys. Rev. Lett.* **87** (2001).
11. D. Oron, N. Dudovich, and Y. Silberberg, "Femtosecond phase-and-polarization control for background-free coherent anti-stokes raman spectroscopy," *Phys. Rev. Lett.* **90** (2003).
12. R. Z. Vered, M. Rosenbluh, and A. Pe'er, "Two-photon correlation of broadband-amplified spontaneous four-wave mixing," *Phys. Rev. A* **86** (2012).
13. T. Jeong and H. S. Moon, "Phase correlation between four-wave mixing and optical fields in double a-type atomic system," *Opt. Express* **24**, 28774 (2016).
14. M. Jurna, J. Kortarik, C. Otto, J. Herek, and H. Offerhaus, "Background free cars imaging by phase sensitive heterodyne cars," *Opt. Express* **16**, 15863–15869 (2008).
15. C. Evans, E. Potma, and S. Xie, "Coherent anti stokes raman scattering interferometry: determination of the real and imaginary components of nonlinear susceptibility," *Opt. Lett.* **29**, 2923 (2004).
16. B. Yurke, S. L. McCall, and J. R. Klauder, "Su(2) and su(1,1) interferometers," *Phys. Rev. A* **33**, 4033–4054 (1986).
17. P. Grangier, R. E. Slusher, B. Yurke, and A. LaPorta, "Squeezed-light enhanced polarization interferometer," *Phys. Rev. Lett.* **59**, 2153–2156 (1987).
18. K. McKenzie, D. A. Shaddock, D. E. McClelland, B. C. Buchler, and P. K. Lam, "Experimental demonstration of a squeezing-enhanced power-recycled michelson interferometer for gravitational wave detection," *Phys. Rev. Lett.* **88** (2002).
19. A. M. Marino, N. V. C. Trejo, and P. D. Lett, "Effect of losses on the performance of an su(1,1) interferometer," *Phys. Rev. A* **86** (2012).
20. M. Manceau, F. Khalili, and M. Chekhova, "Improving the phase super-sensitivity of squeezing-assisted interferometers by squeeze factor unbalancing," *New J. Phys.* **19**, 013014 (2017).
21. M. Manceau, G. Leuchs, F. Khalili, and M. Chekhova, "Detection loss tolerant supersensitive phase measurement with an su(1,1) interferometer," *Phys. Rev. Lett.* **119** (2017).
22. C. M. Caves and B. L. Schumaker, "New formalism for two-photon quantum optics. i. quadrature phases and squeezed states," *Phys. Rev. A* **31**, 3068–3092 (1985).
23. R. Loudon and P. L. Knight, "Squeezed light," *J. Mod. Opt.* **34**, 709–759 (1987).
24. Y. Shaked, Y. Michael, R. Z. Vered, L. Bello, M. Rosenbluh, and A. Pe'er, "Lifting the bandwidth limit of optical homodyne measurement with broadband parametric amplification," *Nat. Commun.* **9** (2018).
25. M. V. Chekhova and Z. Y. Ou, "Nonlinear interferometers in quantum optics," *Adv. Opt. Photonics* **8**, 104 (2016).
26. D. Li, B. T. Gard, Y. Gao, C.-H. Yuan, W. Zhang, H. Lee, and J. P. Dowling, "Phase sensitivity at the heisenberg limit in an su(1,1) interferometer via parity detection," *Phys. Rev. A* **94** (2016).

27. F. Y. Wu, S. Ezekiel, M. Ducloy, and B. R. Mollow, "Observation of amplification in a strongly driven two-level atomic system at optical frequencies," *Phys. Rev. Lett.* **38**, 1077–1080 (1977).
28. J.-X. Cheng, *Coherent Raman Scattering Microscopy* (CRC Press, 2013).
29. G. Marowsky and G. Liipke, "Cars-background suppression by phase-controlled nonlinear interferometry," *Appl. Phys. B* **51**, 49–51 (1990).
30. E. S. Lee, J. Y. Lee, and Y. S. Yoo, "Nonlinear optical interference of two successive coherent anti-stokes raman scattering signals for biological imaging applications," *J Biomed Opt.* **12**, 024010 (2007).
31. R. Z. Vered, Y. Shaked, Y. Ben-Or, M. Rosenbluh, and A. Peařer, "Classical-to-quantum transition with broadband four-wave mixing," *Phys. Rev. Lett.* **114** (2015).
32. S. M. Barnett, J. Jeffers, A. Gatti, and R. Loudon, "Quantum optics of lossy beam splitters," *Phys. Rev. A* **57**, 2134–2145 (1998).
33. L. Bokobza, J.-L. Bruneel, and M. Couzi, "Raman spectroscopy as a tool for the analysis of carbon-based materials (highly oriented pyrolytic graphite, multilayer graphene and multiwall carbon nanotubes) and of some of their elastomeric composites," *Vib. Spectrosc.* **74**, 57–63 (2014).
34. K. L. Gares, K. T. Hufziger, S. V. Bykov, and S. A. Asher, "Review of explosive detection methodologies and the emergence of standoff deep uv resonance raman," *J. Raman Spectrosc.* **47**, 124–141 (2016).